

*This copy is for your personal, non-commercial use only.*

If you wish to distribute this article to others, you can order high-quality copies for your colleagues, clients, or customers by [clicking here](#).

Permission to republish or repurpose articles or portions of articles can be obtained by following the guidelines [here](#).

The following resources related to this article are available online at  
[www.sciencemag.org](http://www.sciencemag.org) (this information is current as of December 2, 2010):

Updated information and services, including high-resolution figures, can be found in the online version of this article at:

<http://www.sciencemag.org/content/317/5837/513.full.html>

Supporting Online Material can be found at:

<http://www.sciencemag.org/content/suppl/2007/07/26/317.5837.513.DC1.html>

This article cites 1 articles, 1 of which can be accessed free:

<http://www.sciencemag.org/content/317/5837/513.full.html#ref-list-1>

This article has been cited by 49 article(s) on the ISI Web of Science

This article has been cited by 24 articles hosted by HighWire Press; see:

<http://www.sciencemag.org/content/317/5837/513.full.html#related-urls>

This article appears in the following subject collections:

Biochemistry

<http://www.sciencemag.org/cgi/collection/biochem>

# Spring-Loaded Mechanism of DNA Unwinding by Hepatitis C Virus NS3 Helicase

Sua Myong,<sup>1,2\*</sup> Michael M. Bruno,<sup>3,4</sup> Anna M. Pyle,<sup>3,4</sup> Taekjip Ha<sup>1,2,4</sup>

NS3, an essential helicase for replication of hepatitis C virus, is a model enzyme for investigating helicase function. Using single-molecule fluorescence analysis, we showed that NS3 unwinds DNA in discrete steps of about three base pairs (bp). Dwell time analysis indicated that about three hidden steps are required before a 3-bp step is taken. Taking into account the available structural data, we propose a spring-loaded mechanism in which several steps of one nucleotide per adenosine triphosphate molecule accumulate tension on the protein-DNA complex, which is relieved periodically via a burst of 3-bp unwinding. NS3 appears to shelter the displaced strand during unwinding, and, upon encountering a barrier or after unwinding >18 bp, it snaps or slips backward rapidly and repeats unwinding many times in succession. Such repetitive unwinding behavior over a short stretch of duplex may help to keep secondary structures resolved during viral genome replication.

In hepatitis C virus (HCV), nonstructural protein 3 (NS3) is an essential component of the viral replication complex that works with the polymerase NS5B and other protein cofactors (such as NS4A, NS5A, and NS2) to ensure effective copying of the virus. The NS3 protein is a bifunctional enzyme that contains both protease and helicase domains (*1–3*) and is unusual in that it can unwind both DNA and RNA substrates (*4, 5*). Unwinding of the highly structured RNA genome of HCV is likely to be the major role for the NS3 helicase; however, it remains possible that activity toward host DNA substrates plays a role in viral function. Indeed, NS3 rapidly binds DNA and unwinds it progressively (*6*). Given these facts and the availability of crystallographic data on NS3-DNA complexes (*7–9*), we sought to elucidate the elementary steps and kinetic mechanisms involved with NS3 unwinding of DNA.

In a previous ensemble study, NS3 was observed to unwind RNA with a physical and kinetic size of ~18 base pairs (bp) (*10*). More recently, single-molecule mechanical studies under assisting force confirmed the periodic nature of RNA unwinding by NS3, but displayed rapid steps of ~3 to 4 bp that were interrupted by long pauses approximately every 11 bp (*11*). These large apparent steps by NS3 contrast with structural studies of other helicases, which suggest that the elemental step for helicase activity is the unwinding of a single base pair, and that this is linked to individual adenosine triphosphate (ATP) hydrolysis events (*12, 13*).

Nonetheless, there are no functional data supporting the existence of unwinding steps of a single base pair each, nor any information on how they might correlate with the larger steps that appear to be involved in the mechanical function of helicase enzymes (*14*).

We used single-molecule fluorescence resonance energy transfer (FRET) to resolve the individual steps of DNA separation catalyzed by NS3 in the absence of applied force. Our standard substrate, PD1, is a partial-duplex DNA (18 bp) with a 3' single-stranded DNA (ssDNA) tail 20 nucleotides (nt) in length. The donor (Cy3) and acceptor (Cy5) fluorophores are attached to the junction through aminodeoxythymidine without interrupting the DNA backbone. The DNA is tethered to a polymer-passivated quartz surface via biotin at the 3' tail terminus (Fig. 1A). After incubation of this assembly with full-length NS3 protein (25 nM) for 15 min, 4 mM ATP solution is flowed into the cell to initiate DNA unwinding. The flow of ATP also serves to remove unbound protein in solution and thereby allows us to monitor unwinding by prebound NS3 (*15*).

After addition of ATP, we observed a FRET decrease that is caused by the increase in the time-averaged (time resolution, 30 ms) interfluorophore distance as the DNA is unwound. The measurements taken at 37°C indicate a rapid FRET decrease that appears to involve intermediate steps (fig. S1). When the temperature was lowered to 30°C to slow the reaction, FRET values decreased with a discrete pattern marked by apparent plateaus corresponding to six steps for unwinding of the 18-bp duplex (Fig. 1, B to E). The same experiment was then performed with an otherwise identical substrate, PD2, in which the fluorophores were relocated 9 bp away from the junction, such that FRET signal is sensitive only to the final 9-bp unwinding (Fig. 1F). Plateaus were also observed in that case, although they occurred with larger FRET increments corresponding to three unwinding steps for

unwinding 9 bp (Fig. 1, G to J). Both sets of data are consistent with a 3-bp unwinding step size. The data also indicate that the two strands do not spontaneously separate when only a few base pairs remain (i.e., via thermal duplex fraying). At the end of each experiment, the displacement of acceptor-labeled strands was confirmed by a direct excitation with a red laser.

To quantify the stepping behavior, we used an automated step-finding algorithm (*16*) (fig. S2), which yielded the average FRET values for each plateau and its dwell time (Fig. 2, A and D). We then built transition density plots (*17*), which represent the two-dimensional histogram for pairs of FRET values before (FRET enter) and after (FRET exit) each transition. Six and three well-isolated peaks emerged for 18-bp and 9-bp unwinding, respectively (about 75 molecules each) (Fig. 2, B and E). The highest FRET peak region (Fig. 2B) appears to be in broader distribution than other peak regions, possibly as a result of the NS3 binding and fluctuating or partially melting the junction and thus slightly separating the two dyes. This analysis shows that there are well-defined FRET states that are visited sequentially during unwinding and that they are each separated by about 3 bp. Similar evidence for 3-bp unwinding steps was found for unwinding an 18-bp duplex of unrelated sequence (fig. S3).

If 3 bp is the elementary step size of unwinding—for example, due to the hydrolysis of a single ATP—the dwell time histogram of the steps would follow a single-exponential decay. In contrast, we obtained nonexponential dwell time histograms that displayed a rising phase followed by a decay (Fig. 2, C and F). If we assume that each 3-bp step requires *n* hidden irreversible Poissonian steps with identical rate *k*, the data can be fit with the gamma distribution,  $t^{n-1} \exp(-kt)$ . The fits gave *n* = 2.84 for 18-bp unwinding and *n* = 2.72 for 9-bp unwinding. The *k* values were 0.78 s<sup>-1</sup> and 0.89 s<sup>-1</sup>, respectively. These rates are similar to the unwinding rate estimated from an earlier bulk solution study of an 18-bp duplex of unmodified DNA (0.66 s<sup>-1</sup> bp<sup>-1</sup>) (*6*). Dwell time histograms built for individual steps gave similar *n* and *k* values for each step (fig. S4). Overall, our data suggest that each 3-bp step is composed of three hidden steps of 1 bp, presumably due to hydrolysis of one ATP each. The emerging model here is that, after three successive ATP hydrolysis events, there occurs an abrupt 3-bp separation.

The helicase domain of NS3 (NS3h), belonging to superfamily 2 (SF2), has three domains. Domain 1 and domain 2 have RecA-like folds, and there is an ATP-binding pocket between the domains. In the crystal structure of NS3h bound to deoxyuridine octamer (dU)<sub>8</sub>, domains 1 and 2 make contacts exclusively to the phosphate-ribose backbone of (dU)<sub>8</sub> with no contact to the bases (*9*). Nonetheless, bases are well resolved in the structure and there is enough room for duplex formation on the 5' side, with only a minor change in the relative position of domain 3.

<sup>1</sup>Physics Department, University of Illinois, 1110 West Green Street, Urbana, IL 61801, USA. <sup>2</sup>Institute for Genomic Biology, University of Illinois, 1206 West Gregory Drive, Urbana, IL 61801, USA. <sup>3</sup>Molecular Biophysics and Biochemistry, Yale University, 266 Whitney Avenue, Room 334A, Bass Building, New Haven, CT 06511, USA. <sup>4</sup>Howard Hughes Medical Institute.

\*To whom correspondence should be addressed. E-mail: smyong@uiuc.edu

The structure, obtained in the absence of ATP, shows that two highly conserved threonines (Thr<sup>269</sup> and Thr<sup>411</sup>) bind to two phosphates that are located 3 nt apart. Mutation of either of these NS3 threonines abolishes unwinding activity (18). By contrast, the Vasa helicase and eIF4AIII structures, determined with adenylyl-imidodiphosphate and 5'-adenylyl-β-γ-imidodiphosphate bound, respectively (19, 20), suggest that domains 1 and 2 will close upon ATP binding and that this would bring the equivalent two threonine residues 2 nt

apart (fig. S5, A to C). This change in the distance between threonine contacts may represent the structural basis for a 1-nt movement: Each ATP binding and product release event is expected to result in the 1-nt movement of domains 1 and 2 in the 3' to 5' direction.

Domain 3 presents a tryptophan (Trp<sup>501</sup>) that is critical for activity. The importance of an aromatic residue at this position is demonstrated by the fact that it can be substituted with phenylalanine, whereas alanine disrupts unwinding (18).

The Trp<sup>501</sup> stacks against the base at the 3' end of (dU)<sub>8</sub> (fig. S5A), which might keep the relative positions of domain 3 and DNA fixed while domains 1 and 2 translocate. This effect would lead to the buildup of tension on both the protein and the DNA, which we propose is released after 3-nt translocation by a sudden movement of domain 3, with concomitant 3-bp unwinding of the DNA (fig. S9).

SF1 helicases such as Rep, UvrD, and PcrA are structurally analogous to SF2 helicases with

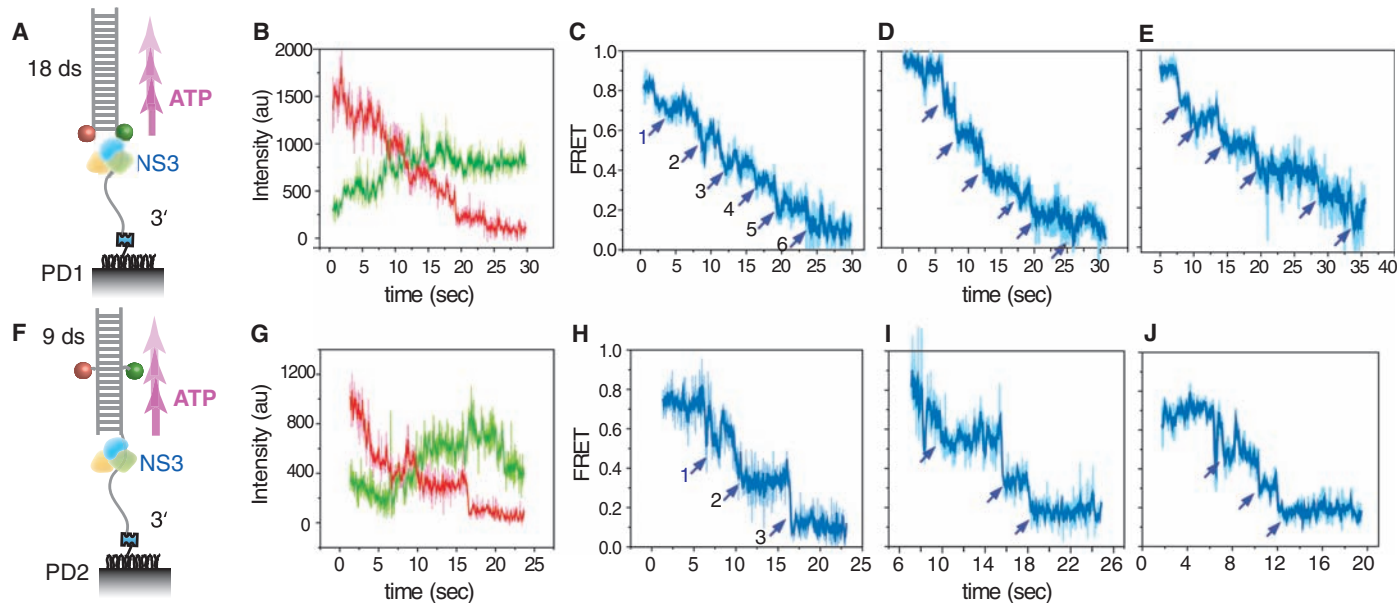
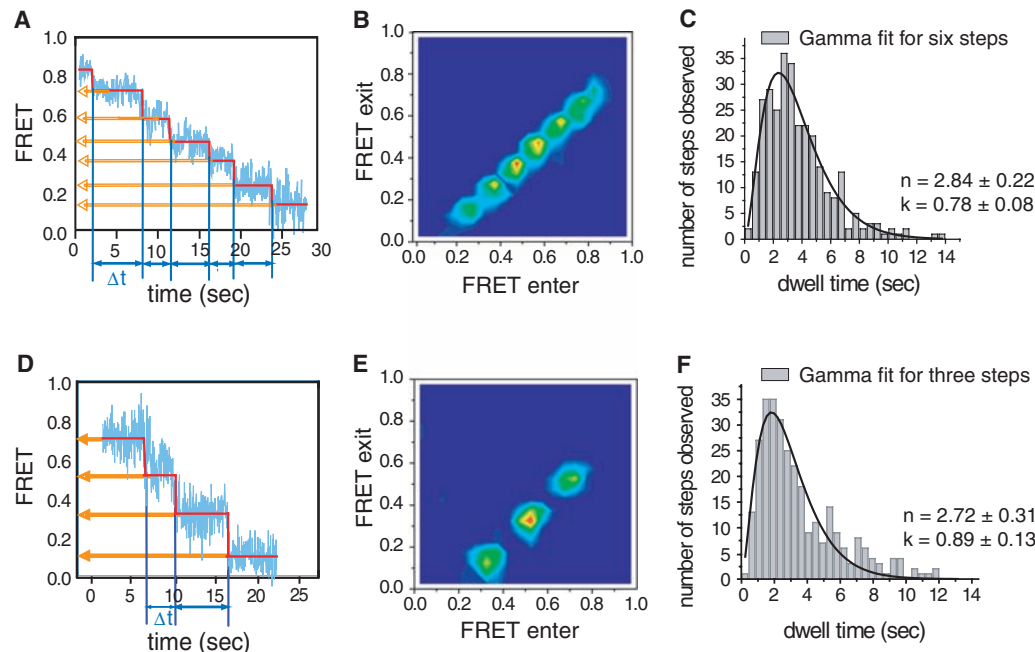


**Fig. 1.** NS3 unwinds DNA in 3-bp steps. **(A)** PD1, a DNA with 18 double strands (ds) and 20 single strands (ss), was labeled with donor (Cy3) and acceptor (Cy5) at the ds-ss junction and was tethered to a polyethylene glycol surface by 3' biotin. **(B)** Cy3 (green) and Cy5 (red) intensities monitored during unwinding of a single PD1 molecule (raw time traces in

light color, three-point averaged traces in dark color). **(C)** Calculated FRET efficiency versus time for the molecule shown in (B). **(D and E)** Two more examples of FRET traces for PD1. **(F)** PD2 is the same construct as in (A) but prepared with dyes in the middle of duplex. **(G to J)** Plots analogous to those in (B) to (E) for PD2.

**Fig. 2.** Each 3-bp step consists of three hidden steps. **(A)** A step-finding algorithm was used to quantify FRET values (orange arrows) and dwell times (blue arrows,  $\Delta t$ ) at each step for a single molecule of PD1. **(B)** FRET values obtained from 75 molecules of PD1 were combined to make a total density plot. **(C)** Gamma distribution fitting of the collected dwell times at each plateau pause duration for PD1 yielded approximately three irreversible steps ( $n$  values) within the 3-bp step, indicating a strong possibility of one nucleotide as an elementary step size. **(D to F)** Plots analogous to those in (A) to (C) for PD2.



superimposable domain arrangement and catalytic site (21, 22). The available crystal structures of these three SF1 helicases all have well-conserved threonine pairs and an aromatic gatekeeper residue, phenylalanine, at the analogous locations to NS3 (fig. S5, D and E). ATP-bound UvrD has the two threonines 2 nt apart, whereas Rep with no ATP shows the threonines 3 nt apart, again supporting the 1-nt movement coupled to one ATP consumption (23).

To observe the unwinding behavior when the duplex end is challenged with a presence of physical blockade, we next examined unwinding of an inverted configuration where the duplex end was tethered to the surface via biotin-streptavidin (Fig. 3A). In this construct we swapped the dye positions so that the donor was attached to the displaced strand and the acceptor on the tracking strand. At 37°C, the same stepwise behavior was observed but the unwinding could not be completed, perhaps because of steric hindrance by the biotin-streptavidin blockade. Some molecules (25%) showed the displaced strand (donor attached strand) remaining in contact with the enzyme for long periods (fig. S6A) after unwinding, whereas many others (75%) displayed a repetitive FRET pattern as shown in Fig. 3B. In most cases, the peaks were asymmetric with an abrupt FRET increase followed by a gradual FRET decrease. We interpret this characteristic

pattern as repeated trials of helicase unwinding followed by rapid rezipping/reannealing of the duplex. Because the unwinding reaction initiated after washing out free protein, such repetition likely arises from one unit rather than the successive binding of different molecules. Could it be that the enzyme bears a secondary binding site that enables it to snap back to restart the next round of unwinding?

We therefore designed a substrate such that the whereabouts of the acceptor-labeled 5' end of the displaced strand could be monitored via FRET from the donor at the duplex end (Fig. 3C). In this experiment, we observed a repeating pattern in the shape of an asymmetric sawtooth where each peak involved a gradual rising phase of FRET followed by an abrupt decrease (Fig. 3D), indicating that the 5' region of the displaced strand is brought close to the duplex end as DNA is unwound. This effect can arise from the enzyme maintaining contact with the 5' region of the displaced strand or from the displaced strand becoming compact because of the flexibility of ssDNA. We prefer the former scenario because of its consistency with the larger FRET changes per step seen for PD2 than for PD1 (Fig. 1). A protein contact with the 5' region of the displaced strand would lead to a looping of the strand, giving rise to a larger distance change per step if the fluorophores are

attached to the middle of the duplex (fig. S7). In this view, the abrupt decrease in FRET may be attributed to NS3 losing its grip on the tracking strand and snapping or slipping back near the junction while maintaining contact with the 5' region of the displaced strand.

On the basis of our findings, we propose the following model for NS3 unwinding of DNA (fig. S9). Domains 1 and 2 of NS3 move along the tracking strand (3' to 5') one nucleotide at a time, consuming one ATP, where ATP binding and ADP release induce closing and opening of the two domains, respectively. The third domain of the protein lags behind by anchoring itself to the DNA until three such steps take place. At the third step, the spring-loaded domain 3 moves forward in a burst motion, unzipping 3 bp as a consequence. The displaced strand is likely to be sheltered by the enzyme instead of being released free. NS3 continues unwinding in 3-bp steps up to about 18 bp unless it encounters an apparent barrier (movie S1). Unwinding performed with duplexes 24 bp or longer showed evidence of repetitive unwinding even when the duplex ends were not blocked (fig. S8), which suggests that NS3 is not highly efficient in going much beyond 18 bp; this is consistent with the reported drop in processivity that is observed every 18 bp in RNA unwinding in bulk solution (10).

The HCV genome is a ~10,000-nt single-stranded RNA that is copied upon binding of the NS3-NS4A-NS5B replicative complex to highly structured terminal untranslated regions (UTRs). Sequence and structural analysis suggests that the UTRs are complex structures comprising short stems and loops (24). The ability of NS3 to maintain contact with displaced strands may provide an advantage by allowing it to stay in a local region to keep RNA stems unwound, because reforming of the secondary structure could hinder viral replication. The repetitive unwinding behavior of NS3 is reminiscent of the repeated translocation observed in Rep (25).

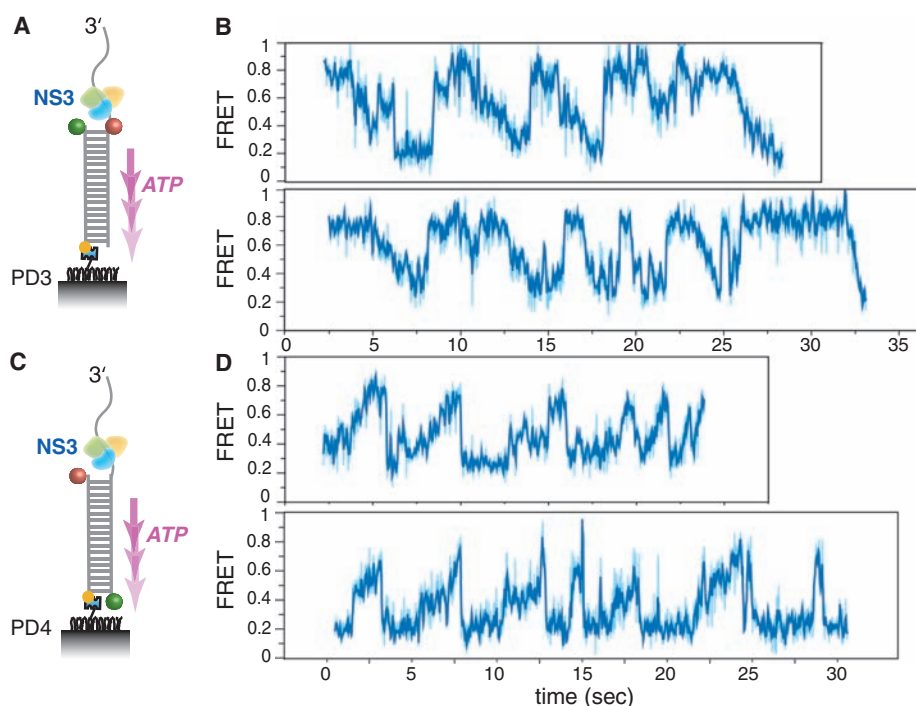


**Fig. 3.** Repetitive unwinding of a short duplex stretch. (A) PD3, a partial duplex with 18 double strands and a tail of 30 single strands, was labeled with cy3 and cy5 at the ds-ss junction and blocked at the duplex end via biotin-streptavidin. (B) A majority of molecules (75%) showed a repetitive unwinding pattern where the enzyme appeared to snap or slip back to near the junction upon encountering a blockade. (C) PD4, a partial duplex with 18 double strands and a tail of 20 single strands, was labeled with cy5 at the ds-ss junction and cy3 at the duplex end. (D) The repetitive cycles of gradual FRET increase followed by rapid FRET decrease indicate that the displaced strand is brought close to the duplex end by NS3, then snaps or slips back to the junction rapidly after encountering the blockade.

#### References and Notes

1. A. M. Di Bisceglie, *Hepatology* **26**, 345 (1997).
2. L. B. Seeff, *Hepatology* **28**, 1710 (1998).
3. D. Lavanchy, *J. Hepatol.* **31** (suppl. 1), 146 (1999).
4. D. W. Kim, Y. Gwack, J. H. Han, J. Choe, *Biochem. Biophys. Res. Commun.* **215**, 160 (1995).
5. C. L. Tai, W. K. Chi, D. S. Chen, L. H. Hwang, *J. Virol.* **70**, 8477 (1996).
6. P. S. Pang, E. Jankowsky, P. J. Planet, A. M. Pyle, *EMBO J.* **21**, 1168 (2002).
7. H. P. Yao, D. J. Xia, L. H. Zhang, K. Z. Liu, *Zhejiang Da Xue Xue Bao Yi Xue Ban* **31**, 2 (2002).
8. L. W. Kang et al., *Acta Crystallogr. D* **54**, 121 (1998).
9. J. L. Kim et al., *Structure* **6**, 89 (1998).
10. V. Serebrov, A. M. Pyle, *Nature* **430**, 476 (2004).
11. S. Dumont et al., *Nature* **439**, 105 (2006).
12. J. Y. Lee, W. Yang, *Cell* **127**, 1349 (2006).
13. M. S. Dillingham, D. B. Wigley, M. R. Webb, *Biochemistry* **39**, 205 (2000).
14. A. J. Ali, T. M. Lohman, *Science* **275**, 377 (1997).
15. See supporting material on Science Online.
16. J. W. Kerssemakers et al., *Nature* **442**, 709 (2006).
17. C. Joo et al., *Cell* **126**, 515 (2006).
18. C. Lin, J. L. Kim, *J. Viral.* **73**, 8798 (1999).
19. T. Sengoku, O. Nureki, A. Nakamura, S. Kobayashi, S. Yokoyama, *Cell* **125**, 287 (2006).

20. C. B. F. Andersen *et al.*, *Science* **313**, 1968 (2006); published online 23 August 2006 (10.1126/science.1131981).
21. K. J. Marians, *Structure* **5**, 1129 (1997).
22. S. Korolev, N. Yao, T. M. Lohman, P. C. Weber, G. Waksman, *Protein Sci.* **7**, 605 (1998).
23. E. J. Tomko, C. J. Fischer, A. Niedziela-Majka, T. M. Lohman, *Mol. Cell* **26**, 335 (2007).
24. M. Houghton, A. Weiner, J. Han, G. Kuo, Q. L. Choo, *Hepatology* **14**, 381 (1991).
25. S. Myong, I. Rasnik, C. Joo, T. M. Lohman, T. Ha, *Nature* **437**, 1321 (2005).
26. We thank C. Joo for help in manuscript preparation. Supported by NIH grants R01-GM060620 and R01-GM065367. T.H. and A.M.P. are investigators with the Howard Hughes Medical Institute.

**Supporting Online Material**[www.sciencemag.org/cgi/content/full/317/5837/513/DC1](http://www.sciencemag.org/cgi/content/full/317/5837/513/DC1)

Materials and Methods

Figs. S1 to S9

Movie S1

23 April 2007; accepted 26 June 2007

10.1126/science.1144130

# Sirtuin 2 Inhibitors Rescue $\alpha$ -Synuclein–Mediated Toxicity in Models of Parkinson’s Disease

Tiago Fleming Outeiro,<sup>1,2</sup> Irene Kontopoulos,<sup>3\*</sup> Stephen M. Altmann,<sup>2\*</sup> Irina Kufareva,<sup>4</sup> Katherine E. Strathearn,<sup>5</sup> Allison M. Amore,<sup>2</sup> Catherine B. Volk,<sup>5</sup> Michele M. Maxwell,<sup>2</sup> Jean-Christophe Rochet,<sup>5</sup> Pamela J. McLean,<sup>1,2</sup> Anne B. Young,<sup>2</sup> Ruben Abagyan,<sup>4</sup> Mel B. Feany,<sup>3</sup> Bradley T. Hyman,<sup>1,2</sup> Aleksey G. Kazantsev<sup>2†</sup>

The sirtuins are members of the histone deacetylase family of proteins that participate in a variety of cellular functions and play a role in aging. We identified a potent inhibitor of sirtuin 2 (SIRT2) and found that inhibition of SIRT2 rescued  $\alpha$ -synuclein toxicity and modified inclusion morphology in a cellular model of Parkinson’s disease. Genetic inhibition of SIRT2 via small interfering RNA similarly rescued  $\alpha$ -synuclein toxicity. Furthermore, the inhibitors protected against dopaminergic cell death both in vitro and in a *Drosophila* model of Parkinson’s disease. The results suggest a link between neurodegeneration and aging.

**A**ging is a major risk factor for the development of several neurodegenerative diseases, including Parkinson’s disease (PD). Although the molecular basis of aging is yet to be determined, biological pathways involved in aging may provide targets for therapeutic intervention in neurodegeneration. PD causes loss of dopaminergic neurons and development of Lewy bodies containing  $\alpha$ -synuclein ( $\alpha$ -Syn) in the substantia nigra (1). Allele multiplication and mutations link  $\alpha$ -Syn to familial forms of PD (2).

Silent information regulator 2 (Sir2), a nicotinamide adenine dinucleotide-dependent histone deacetylase (HDAC) in yeast, participates in numerous cell functions including cell protection and cell cycle regulation (3). The sirtuins are evolutionarily conserved, and seven distinct sirtuin proteins, SIRT1 to SIRT7, have been identified in humans. The mammalian ortholog of yeast Sir2, SIRT1, is up-regulated under conditions of caloric

restriction and resveratrol treatment and is predicted to have a role in cell survival (4). Human SIRT2 is involved in cell cycle regulation via the deacetylation of  $\alpha$ -tubulin (5). However, the iden-

tification of p53 and histones H3 and H4 as additional substrates for SIRT2 suggests a broader regulatory role in the cell (6, 7). Small-molecule inhibitors targeting HDACs ameliorate several models of neurodegeneration (8).

Compound B2 is associated with an increase in intracellular  $\alpha$ -Syn inclusion size from numerous small aggregates to larger inclusions (9). B2 activity was examined in a panel of cell-free enzymatic assays including HDAC I and II; SIRT1, 2, and 3; caspase 1 and 6;  $\beta$ -site amyloid precursor protein cleaving enzyme-1 (BACE1); calpain; cathepsin H, L, and S; and molecular chaperones Hsp70 and Hsp27. The only activity detected was a weak [median inhibitory concentration ( $IC_{50}$ ) = 35  $\mu$ M], but consistent, selective inhibition of SIRT2 (Fig. 1, A and B, and fig. S1). To determine the relevance of SIRT2 inhibition, we used a targeted knockdown approach. Human neuroglioma cells (H4) were cotransfected with  $\alpha$ -Syn expression constructs and synthetic small interfering RNA (siRNA) against either SIRT2 or SIRT3 for 24 hours and were then assessed for cytotoxicity. Rescue of  $\alpha$ -Syn-mediated toxicity was observed only in cells receiving the SIRT2

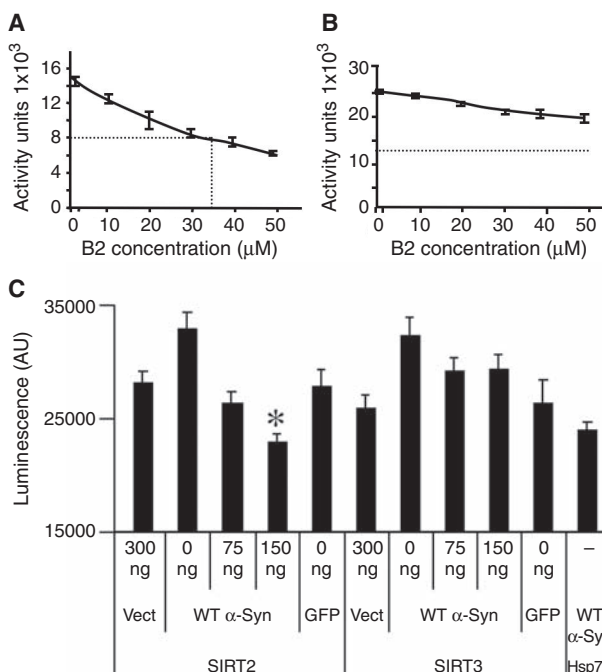


**Fig. 1.** Inhibition of SIRT2 modulates  $\alpha$ -Syn toxicity. (A and B) B2 biochemical activity profiles against SIRT2 (A) and SIRT3 (B) in an in vitro deacetylation biochemical assay containing recombinant SIRT proteins. (C)  $\alpha$ -Syn-mediated toxicity can be rescued with SIRT2 siRNA and Hsp70 overexpression but not with SIRT3 siRNA in vitro (*t* test,  $n = 3$ , \* $P < 0.005$ ).

\*These authors contributed equally to this work.

†To whom correspondence should be addressed. E-mail: [kazantsev@partners.org](mailto:kazantsev@partners.org)